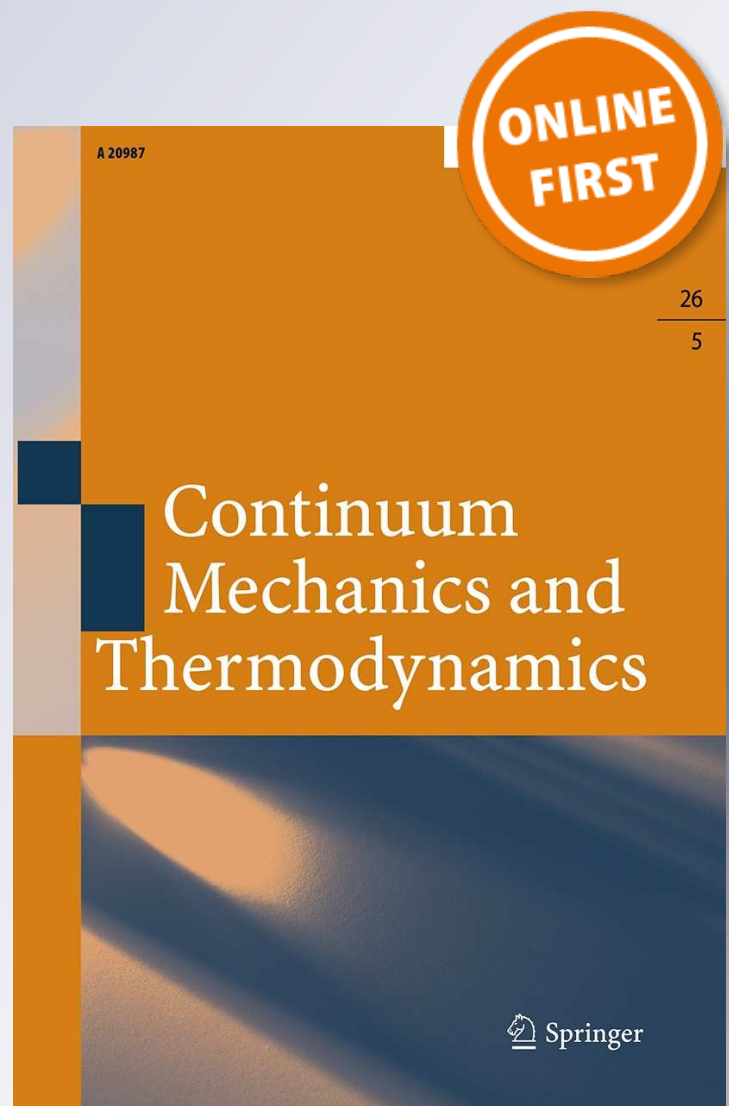# Resonant phase dynamics in 0-π Sine–Gordon facets

Giacomo Rotoli, Daniela Stornaiuolo, Karin Cedergren, Antonio Leo, Thilo Bauch, Filomena Lombardi & Francesco Tafuri

A 20987

ONLINE FIRST

26
5

Continuum
Mechanics and
Thermodynamics

Springer

Springer

Springer

ORIGINAL ARTICLE

**Giacomo Rotoli · Daniela Stornaiuolo · Karin Cedergren ·
Antonio Leo · Thilo Bauch · Filomena Lombardi ·
Francesco Tafuri**

Resonant phase dynamics in 0-π Sine–Gordon facets

Abstract A locally phase-shifted Sine–Gordon model well accounts for the phenomenology of unconventional Josephson junctions. The phase dynamics shows resonant modes similar to Fiske modes that appear both in the presence and in the absence of the external magnetic field in standard junctions. In the latter case, they are also in competition with zero field propagation of Sine–Gordon solitons, i.e., fluxons, which give rise to the so-called zero field steps in the current–voltage (I–V) of the junction. We numerically study the I–V characteristics and the resonances magnetic field patterns for some different faceting configurations, in various dissipative regimes, as a function of temperature. The simulated dynamics of the phase is analyzed for lower-order resonances. We give evidence of a nontrivial dynamics due to the interaction of propagating fluxons with localized semifluxons. Numerical results are compared with experimental outcomes obtained on high-quality high-Tc grain boundary YBCO junctions.

Keywords Sine–Gordon equation · Josephson effect · Fluxons

1 Introduction

Among strongly nonlinear partial differential equations describing physical objects, there are several examples of completely integrable systems, which include dissipative effects and temperature to describe real-world systems [1,2]. Dissipative effects appear both in first derivative terms [3], breaking the time-reversal invariance, and as noise terms, making the model amounts to a Langevin (stochastic) dynamics. The perturbed Sine–Gordon (PSG) model [4] has been for a long time strictly linked to the long Josephson junction (LJJ) model, i.e., a

G. Rotoli (✉)
Dipartimento di Ingegneria Industriale e dell'Informazione, Seconda Università di Napoli, Aversa, CE, Italy
E-mail: giacomo.rotoli@unina2.it; giacomo.rotoli@gmail.com

D. Stornaiuolo
CNR-SPIN e Dipartimento di Scienze Fisiche, Universitá di Napoli "Federico II", via Cinthia, 80125 Naples, Italy

K. Cedergren · T. Bauch · F. Lombardi
Department of Microelectronics and Nanoscience, Chalmers University of Technology and Göteborg University,
41296 Gōteborg, Sweden

A. Leo
CNR-SPIN and Dipartimento di Fisica E R Caianiello, Universitá di Salerno, Via Ponte Don Melillo, 84084 Fisciano, SA, Italy

F. Tafuri
CNR-SPIN and Dipartimento di Ingegneria Industriale e dell'Informazione, Seconda Università di Napoli, Aversa, CE, Italy

junction whose physical length L is larger than the Josephson length λ_J [5,6]. In this approach, SG-solitons are called fluxons, because they carry a flux quantum $h/2e$ and "perturbation" includes dissipative terms and noise, which affect the fluxon's propagation. Fluxons appear in many configurations involving Josephson junctions as discrete one-dimensional [7] or two-dimensional [8,9] arrays of Josephson junctions (JJA), or long junctions coupled via lumped elements [10]. Models of granular superconductors also involve disordered JJA [11,12]. In this last decade, the PSG model has been revisited introducing a local region where a phase shift is present, i.e., $\sin(\varphi)$ is replaced by $\sin(\varphi + \theta)$, the gauge invariant difference $\varphi(x, t)$ is the solution of PSG equation, and θ is a constant in a given region called a "facet." These facets connect at discontinuity points giving rise to a nonlinear stress region, which is found in many one-dimensional nonlinear models with imperfections [13,14]. This occur because each facets can be roughly considered as a pendulum [15] with a different direction of vertical axis. We focus on the case $\theta = \pi$, i.e., the so-called π-junction, which is the most common experimental condition. Pioneering studies refer to the simple two facets structure [16], showing the presence of a localized soliton, called semifluxon which carries a half-flux quantum, pinned at the discontinuity point between two facets. Later the PSG model has been extended to the case of many facets [17]. The static configurations of the phase difference $\varphi(x)$ where x is the coordinate along the facets have been widely investigated [18]. The presence of half-flux quanta has been demonstrated in 1d and 2d arrays of engineered faceted junctions [19,20]. Various configurations of semifluxons along the junction may arise depending on the number of the facets and their length. Annular configurations have been also considered [21,22]. Earlier analysis of phase dynamics [23–25] has also shown that the semifluxon has its proper dynamics, i.e., it can 'flip' between the up state ↑, an anticlockwise localized spontaneous current, and down state ↓, a clockwise localized spontaneous current [24]. However, several aspects of the dynamical states in faceted junctions have still to be analyzed. It has to be clarified, for instance, whether the step voltage structures, often observed [26–29] in the I–V characteristics of high-Tc junctions, can be ascribed to dynamical resonant states or not. The semifluxons flip dynamics can give rise to a rearrangement of the semifluxon chain along the junction in the presence of a bias current. This implies that, depending on the initial configuration of semifluxons along the junction, the magnetic field pattern is no longer symmetric and the dynamical switch between stable configurations can drive the junction into a resistive state.

In the conventional PSG model, two kinds of resonances have been reported: current singularities, zero field steps (ZFS), which appear in the absence of an external magnetic field, and Fiske steps (FS), which arise when a magnetic field is externally applied via boundary conditions to the system [30,31]. Two different resonance dynamics have been suggested to explain the presence of current singularities. First, in long junctions, fluxons shuttle back and forth along the junction [32], generating ZFS. In a junction of normalized length $l = L/\lambda_J$, the normalized voltage positions of the ZFS are given by $V_k = 2k\pi/l$. On the other hand, FS are generated by interaction of e.m. cavity modes with the ac Josephson effect. The theory developed by Kulik [33], based on the excitation of e.m. standing waves, is in good agreement for most of the experimental observations of Fiske steps in small junctions. FS appear at the normalized voltage positions $V_k = k\pi/l$, where k is an integer number. Thus, the normalized voltage for even order FS coincides with ZFS voltage. Second, a different explanation is based on the observation that an external magnetic field causes an asymmetric phase dynamics through the boundary conditions. The fluxon propagation becomes unidirectional: fluxons enter from one side of the junction and annihilate on the opposite one. According to this hypothesis, sometimes referred to as "Samuelsen hypothesis" [34,35], the fluxon propagation is responsible also for existence of FS, besides ZFS, in long junctions.

Cirillo et al. [36] have made evident that two separate regimes in long junctions depend on the intensity of the applied magnetic field. At small fields, the fluxon picture applies. For larger fields, i.e., beyond the threshold represented by Tinkham field $H_0 = 2\lambda_J J_0$ [37], the field penetrates into the junction and the dynamics is dominated by a cavity mode mechanism as far as its magnetic properties are concerned. In the extended version of PSG model, able to account for the facets in the barrier, the phase dynamics is more complex due to the presence of intrinsic magnetic field created by the spontaneous currents. For example, for an even number N of facets (with equal length) in zero magnetic field, a family of resonances similar to ZFS appear at voltages $V_k = k\pi/l$ with k odd (half-integer ZFS, or ZFSk/2). For two facets, $N = 2$, this dynamics has been reported in Ref. [23] in the case of very low dissipation. The behavior is characterized by the presence of localized magnetic moments of semifluxons that amounts to a local magnetic field and gives rise to a FS dynamics in zero field. On the other hand, for an odd number of equal facets, the local magnetic field of an equal number of semifluxons does not carry a net magnetic moment and ZFS appear at the usual voltages $V_k = k\pi/l$ with k even; thus, also Fiske steps of even order appear. These observations have been very recently also demonstrated in experiments [38] for the case of a $N = 2$ facets ferromagnetic tunnel Josephson junction.

Four questions summarize the main issues: (1) Are these dynamics still due to the propagation of quasi-solitonic modes (fluxons) and to their interaction with localized semifluxons? If this is not the case, is the dynamics rather described on the basis of the e.m. cavity modes, as in conventional junction, because of the presence of spontaneous magnetic moments? (2) How is the dynamics influenced by the faceting parity (N odd or even)? (3) What is the temperature dependence of these dynamical states? (4) Finally, what is the difference between a junction characterized by a perfect (engineered) distribution of facets lengths, and a junction with a random distribution of facets lengths?

Other related issues are the role of the junction normalized size l and of dissipation in determining the nature of resonances observed in I–V characteristics. For sake of brevity, here we shall not consider very long junctions ($l > 10$) except in some particular cases. In fact, very long high-T_c junctions will have a too high dissipation to show a fully resonant dynamics [39].

The numerical analysis of I–V leads to a systematic study of resonances and their magnetic field pattern for the different configurations. When an external magnetic field is applied, the resonances show a characteristic interference pattern. The magnetic field pattern turns out to be crucial to determine the order and the nature of the resonance. Different underlying dynamics can produce side-lobes in the resonance magnetic field pattern that can be identified as competition between e.m. cavity modes and fluxon propagation. We confine our study to some cases that can be more directly compared with experiments.

The study of the resonances appearing in the I–V characteristics by numerical simulations answers the main questions above. Most of the values of the parameters used in the simulations will be inspired by the estimates in high critical temperature superconductors (HTS) YBCO biepitaxial "grain boundary" junctions that can be naturally faceted. Below, we report some experimental measurements from two different junctions, a corner and a submicron biepitaxial junction, respectively. The behaviors reflect the different morphologies.

The paper is organized as follows: in Sect. 2, we briefly describe the model of long faceted Josephson junction and our numerical approach; in Sect. 3, we report the I–V characteristics and the magnetic field dependence of several resonances for different facets numbers and configurations. In Sect. 4, a comparison with experiments is carried, and finally, some conclusions are presented in Sect. 5.

2 Model

Dynamics of gauge invariant phase difference $\varphi(x, t)$ along the GB faceted junction extended in the x direction can be simulated using the PSG model in presence of 0-π facets [16] with a spatially dependent $j(x)$ current density. A sketch of a faceted Josephson junction is reported in Fig. 1a, b. For long GB junction of physical length L, the Sine–Gordon equation for the phase difference $\varphi(x, t)$ is written as [18]:

$$\varphi_{tt} - \varphi_{xx} + \alpha\varphi_t + \varepsilon(x)\sin\varphi = \gamma + \gamma_N \tag{1}$$

with boundary conditions given in terms of normalized magnetic field η:

$$\varphi(0, t) = \varphi(l, t) = \eta$$

In Eq. (1), time is normalized to (zero bias) plasma frequency $\omega_J = \sqrt{2\pi I_0/C\Phi_0}$ (I_0 is the critical current and Φ_0 is the flux quantum) and the lengths to the Josephson penetration depth $\lambda_J = \sqrt{\Phi_0/2\pi\mu_0 dJ_0}$ where $J_0 = I_0/Lw = (1/Lw)\int_0^L |j(x)|dx$ is the mean absolute value of critical current density and d is the magnetic thickness of junction $d = 2\lambda_L + t$, λ_L is the London length, t the barrier thickness and w the junction width. $\eta = (2\pi\mu_0\lambda_L\lambda_J/\Phi_0)B$ is the normalized magnetic field. In Eq. (1), α is the normalized normal conductance, i.e., $\alpha = 1/Q = 1/\sqrt{\beta_C}$, where $\beta_C = 2\pi I_0 R^2 C/\Phi_0$ is the Stewart–McCumber parameter and $\gamma = I_b/I_0$ the normalized bias current, respectively [40,41]. Finally, γ_N is a dimensionless noise current with Gaussian autocorrelation function:

$$\langle\gamma_N(x, t)\gamma_N(x', t')\rangle = \frac{4\pi l\alpha k_B T}{\Phi_0 I_0}\delta(x - x')\delta(t - t').$$

The coefficient $\varepsilon(x) = j(x)/J_0$ is related to the current distribution and is positive for conventional facets and negative for π facets. We suppose that facets have different lengths, i.e., for a normalized junction length l, we consider a partition $\{a_1, a_2, a_3, \ldots a_N\}$ of l in N different facets such that $\sum_j^N a_j = l$. In the following by "perfect" (symmetric) faceting, we mean that all a_j are equal, i.e., $a_j = a$ for any j (see Fig. 1a). The other interesting case is the "random" faceting in which the a_j are extracted by a random statistical population (see
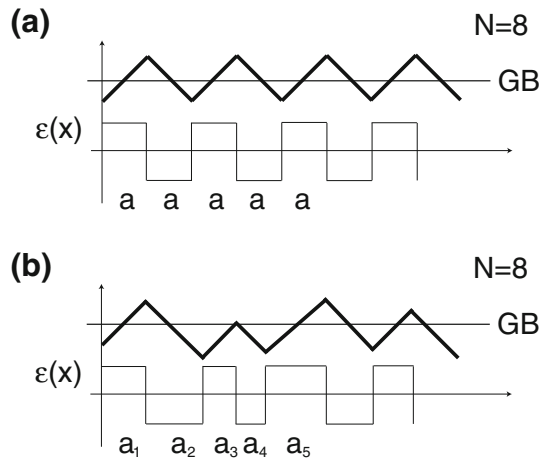
Fig. 1 a A sketch of a faceted Josephson junction in the perfect faceting case, **b** a sketch of a faceted Josephson junction in the random faceting case

Fig. 1b). Without loss of generality here, we suppose that $|j(x)|/J_0 = 1$, because a difference in the absolute value of conventional and π current in a given facet can always be modeled by a different facet normalized lengths [42].

We do not study here the random faceting case. We limit ourselves to note that the analysis of the random faceting, arising from a population of N facets, is related to the fluctuation dissipation theorem and to the Langevin's equation, and generally implies that the noise current autocorrelation is not trivial. In particular, it has been recently shown [43] that in the case of a population of facets with finite N, although large, the dependency between the Langevin equation and the fluctuation dissipation theorem can be approached in a perturbation context in terms of the small parameters $1/N$. Therefore, instead of Eq. (1), a cascade of similar Langevin-like equations can be considered.

Equation (1) can be used to find the I–V characteristic of the junction, ramping the current bias from zero and calculating the average voltage $V = \langle \varphi_t \rangle$. In Sect. 4, we show that the simulations reproduce with good accuracy the experimental results for a dissipation parameter in the interval $0.1 < \alpha < 0.2$ in agreement with the hysteretical behavior of I–V curve. Such range of values of α is compatible with (relatively) low values of dissipation observed in hysteretical bi-epitaxial junctions [27,44,45]. In the simulations, we start from the lowest energy semifluxons configuration, e.g., the anti-ferromagnetic state $\uparrow\downarrow\uparrow \cdots \downarrow\uparrow$ which is the minimum energy state for a faceted junction at zero bias current [46]. This state is doubly degenerate with its reversed semifluxons state $\downarrow\uparrow\downarrow \cdots \uparrow\downarrow$. For an odd number of semifluxons, or N even, the interaction with an external field removes the degeneracy, giving rise to asymmetries in critical current patterns, as will be discussed below.

3 Magnetic field patterns

In Figs. 2 and 6, we report the magnetic field patterns of both critical current and resonances for a conventional LJJ with $l = 5$ (Fig. 2) and for perfectly faceted long junctions with $l = 5$ and $N = 2, 3$ (Figs. 3, 4), respectively. The 2d plots have been obtained by calculating the dynamical differential resistivity $R_d = dV/d\gamma$ to observe the complete behavior of both the critical current and the resonances of the junction as function of the variables γ_b (bias current) and η (magnetic field). Each of the bright region or bright spots (high R_d) in the Figs. 2 and 4 corresponds to a switch between dynamical states. Thus, bright regions or bright spots mark the pattern boundary of critical currents and resonances. By converse, region of very low or zero resistance, critical currents and steps appears as darker areas (blue online). The background light gray (green online) corresponds to the resistive state with $R_d \sim 1/\alpha$ in normalized units. The critical current pattern is in the front in dark gray (dark blue online) with zero R_d, and resonances appear as regions of very low R_d developing over resistive background and going over the grayscale (blue to cyan online). Experimental results on biepitaxial YBCO GB Josephson junctions suggest the values of normalized length and dissipation used in the simulations shown below. We set $l = 5$, and $\alpha = 0.2$, which also satisfy the criterium for a resonant dynamics [39].

Whenever the hysteresis causes the critical current and resonances patterns overlap each other, we start the simulation at high bias where the junction is in a flatly rotating state (the so-called McCumber state), then
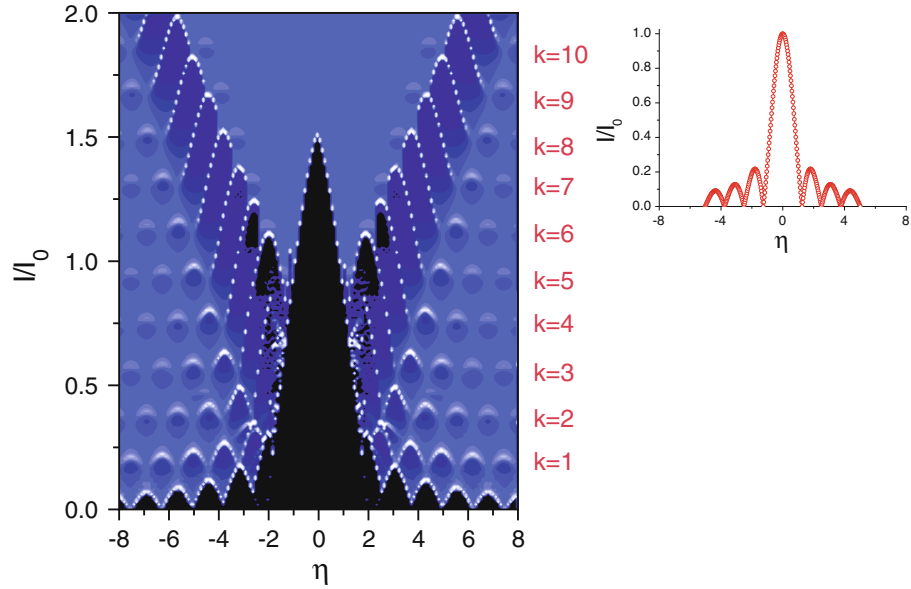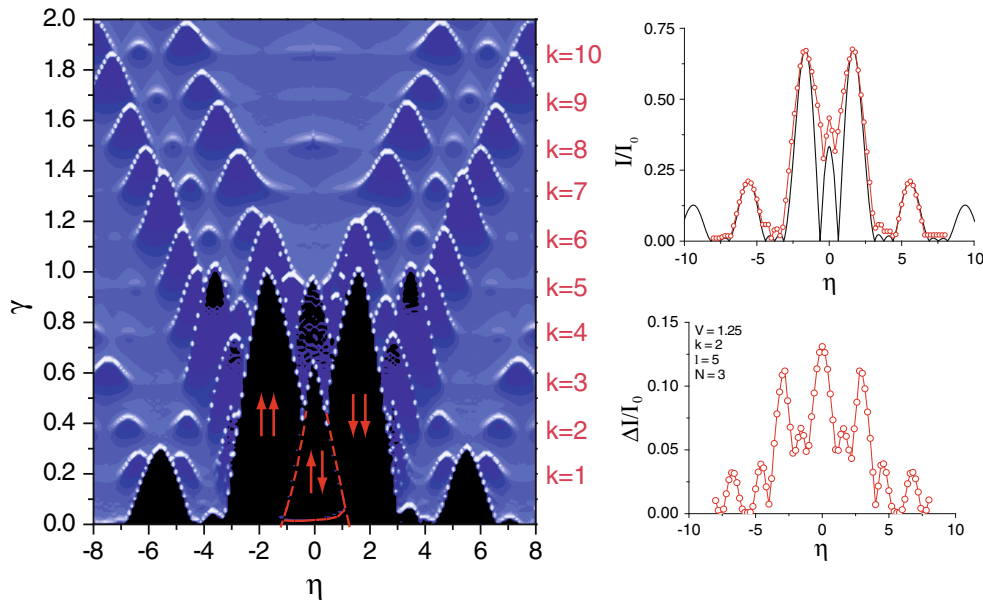
Fig. 2 2D plot of dV/dI as function of normalized current and magnetic field for zero faceting (conventional junction, $N = 1$) and $\alpha = 0.2$, $l = 5$. In the *inset*, the critical current magnetic field pattern obtained from simulations (*circles*) and Eq. (2) (*full line*)
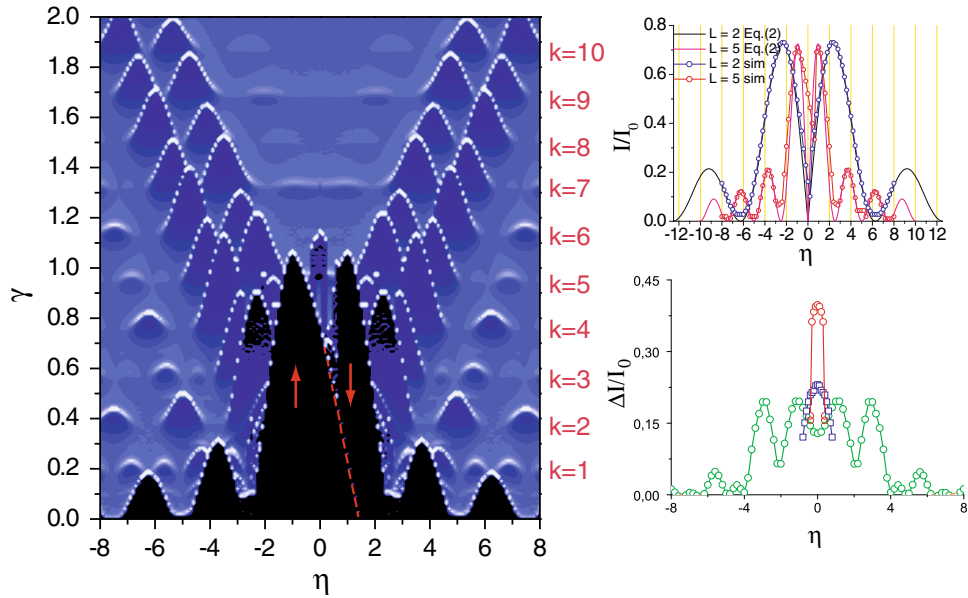
Fig. 3 2D plot of dV/dI as function of normalized current and magnetic field for perfect faceting and $\alpha = 0.2$, $l = 5$ and $N = 2$. Darker areas represent regions of low dynamical resistance. Semifluxons static configurations and their "flip" lines have been marked in *red* to help the reader. In the *top inset*, the critical current versus magnetic field is reported for $l = 2$ and $l = 5$ (*lines with circles*). The *full line* is the result of Eq. (2). In the *bottom inset* is reported the magnetic field behavior of first two resonances $k = 1$ (*squares*) and $k = 3$ S (*empty circles*) and F (*full circles*) branches (color figure online)

decrease the bias until the average voltage V is close to the resonance we want study and finally, increase again the bias to determine the pattern. We use this technique to derive some patterns for single resonances shown in the insets at right of 2d plot. We comment on each of them in the following.

The most prominent feature in Figs. 2 and 4 is the critical current pattern that we describe in subsection A below; in subsection B, we discuss the step structure at finite voltages.

Fig. 4 2D plot of dV/dI as function of normalized current and magnetic field for perfect faceting and $\alpha = 0.2$, $l = 5$ and $N = 3$. *Darker areas* represent regions of low dynamical resistance. In the *top inset*, the critical current magnetic field pattern is reported for $l = 5$ (*lines with circles*). The *full line* is the result of Eq. (2)
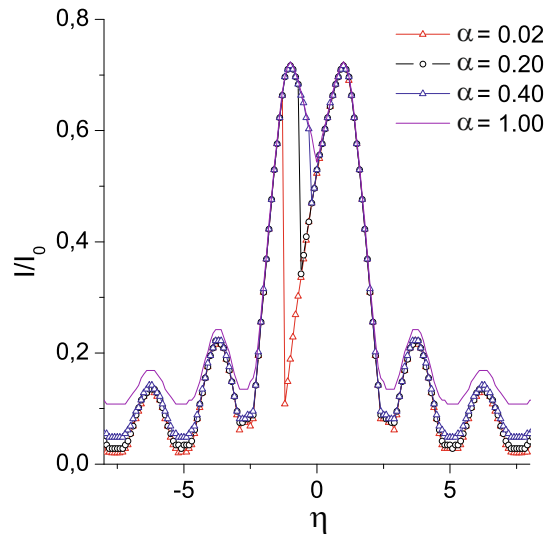
3.1 Critical current patterns

The envelope of numerically simulated pattern, i.e., the maximal critical current at a given field, can be compared with the analytical expression given in Refs. [19,20] in normalized units:

$$I(f) = \frac{1}{2\pi f} \sqrt{\left(\sum_{n=1}^{N}(\chi \sin \zeta_n - \xi \cos \zeta_n)\right)^2 + \left(\sum_{n=1}^{N}(\chi \cos \zeta_n + \xi \sin \zeta_n)\right)^2} \qquad (2)$$

where $\zeta_n = n(\pi - 2\pi f/N)$, $\chi = 1 - \cos(2\pi f/N)$, $\xi = \sin(2\pi f/N)$ and $f = \Phi/\Phi_0 = \eta l/2\pi$ with Φ the magnetic flux coupled to the junction. This formula is substantially confirmed by numerical simulations for different values of N (see the top right insets in Figs. 2 and 4 where both $l = 2$ and $l = 5$ patterns are reported). For $N = 1$, Eq. (2) reduces to conventional Fraunhofer pattern as it is evident in Fig. 2 and in its top right inset. For large values of $l \sim 10$, independently of N, critical current patterns collapse in a single peak and the lateral lobes merge in an uniform structure [40]. This happens in conventional long junctions as well. For $l > \pi$, the central peak of magnetic field pattern occurs for $|\eta| < 2$, which corresponds in physical units to the so-called Tinkham field $H_0 = 2J_0\lambda_J$, i.e., the field for the complete magnetic penetration of the junction [31]. The numerically simulated pattern for a generic facet number N is build up of many subpatterns, each belonging to a different semifluxon configuration in the junction (whenever the identification is possible, we report the semifluxon configuration in the inset plots using the arrows notation: ↑ and ↓ indicate semifluxon of different polarities, respectively).

The merit of a numerical approach is also to enlighten transition between configurations of the phase in the junction, transitions that Eq. (2) cannot predict. This is a new dynamical effect, absent in conventional LJJs due to the rearrangement of static patterns of semifluxons. At low dissipations, some phase configurations become unstable and produce a switch of the whole junction to a resistive state before critical current is reached.

For example, we see from Fig. 3, both in the main plot and in the top inset, that for $N = 2$ and $l = 5$, the pattern is asymmetric reflecting the starting polarity ↑ of the single semifluxon in the junction. The critical current pattern is shown in the top right inset of Fig. 3. The continuous symmetric curve is the prediction of Eq. (2). We again see that for $l = 5$, the simulated pattern is asymmetric reflecting the semifluxon initial polarity. Moreover, a sort of faint "flip line" made of bright spots separates the two states. It corresponds to the presence of a voltage spike due to a dynamical flip between the two states or a resistive switch.

Fig. 5 Critical current magnetic field pattern dependence on dissipation α for $l = 5$, $N = 2$ and semifluxon prepared $\uparrow$

The "paramagnetic" solution, i.e., the polarity of the (odd) semifluxon having the same sign of the magnetic field [17], becomes unstable at lower bias current with respect to "diamagnetic" solution, i.e., opposite sign of the magnetic field and the semifluxon. This lowest "critical" current is marked by the flip line. When the flip line is reached, the semifluxon can either flip in the opposite polarity or the whole junction can reach a resistive state. The reverse asymmetry is obtained with the opposite polarity, $\downarrow$.

The switch to the resistive state is more easily observed at low dissipation, and thus, the visibility of the asymmetry depends on the dissipation, as is clearly evident from difference in the pattern dip between $\alpha = 0.2$ and $\alpha = 1.0$ (see Fig. 5 for the pattern dependence on α). In the $\alpha = 1.0$ case, the dip in the pattern looks less evident, because after the flip the high dissipation prevents the junction from reaching the resistive state. However, the flip line under the right side of the pattern is again visible due to voltage fluctuations excited by flip dynamics, which reduce the dynamical resistance. The asymmetry of the pattern may be not observable if the junction is prepared randomly at 50 % in the each of two polarities $\uparrow$ and $\downarrow$, because the resulting pattern will be an average of two specular asymmetric patterns, but the center dip is always present as well as two flip lines.

For $N = 3$ and $l = 5$, the critical current pattern is symmetric (see Fig. 4). In general, this occurs for any odd value of N. The flip lines visible in the pattern are due to the transition from anti-ferromagnetic $\uparrow\downarrow$ to ferromagnetic $\uparrow\uparrow$ (or $\downarrow\downarrow$) configurations by flipping the semifluxon, which is opposite to field. Thus, the large symmetric lobes belong to a ferromagnetic configuration. The well-marked "flip" lines present in central lobe, at small bias current, are due to initial preparation in $\downarrow\uparrow$ state, which is stable only for small positive current due to semifluxons instability near the ferromagnetic solutions (the reverse occurs for negative currents).

3.2 Resonances patterns

In the resonance patterns, we can identify three different types of structures corresponding to different dynamics model:

1. Fiske Step resonances (FS). In analogy to conventional LJJ reported in Fig. 2 ($N = 1$), the resonance patterns of faceted junctions of Figs. 3, 4 and 6 ($N = 2, 3, 5, 6$) show maxima at progressively larger magnetic field, marking on the 2d plots two *wings* where most significant resonances are found. This structure is related to the step order which is indicated at left of main picture in Figs. 2 and 4. For the conventional junction in Fig. 2, the wings follow a "Bessel function behavior" like in small junction. In Figs. 3, 4 and 6, the presence of faceting generates two 'sub-wings' structures in the central part of the pattern, which arise from the critical current pattern maxima and show maxima shifting toward *lower* magnetic fields.

2. ZFS for $k \leq N$. In Figs. 3, 4 and 6, structures occurring near zero field could be identified as the equivalent of ZFS in conventional junctions, i.e., dynamics on these resonances is dominated by (free)
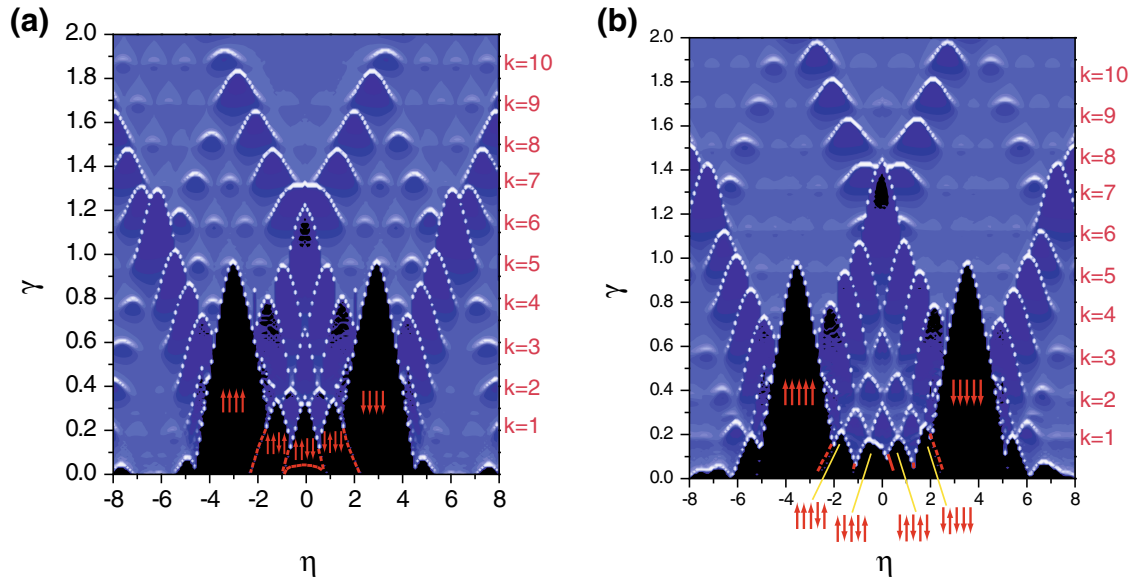
Fig. 6 2D plot of dV/dI as function of current and magnetic field for perfect faceting and $\alpha = 0.2$, $l = 5$ and $N = 5, 6$. The *arrows* indicate the semifluxon configurations in the junction

fluxon propagation, as we will show below. As general rule, it is observed that for even N, e.g., $N = 2, 4$ in Figs. 3 and 6b, the pattern of k odd steps will show a finite ZFS. This is different from conventional systems where the ZFS's are present only for even k. In faceted junction with even N, we do not observe ZFS for even k in our simulations. ZFS resonances give rise to complex pattern for higher N. In Fig. 6 for $N = 5, 6$, the 'sub-wings' cross at the order $k = N - 1$ where a large ZFS step is observed. In Fig. 6, they appear at the orders $k = 4$ (ZFS2) and $k = 5$ (ZFS5/2), respectively. It emerges that when the number of semifluxons $(N - 1)$ matches the number of fluxons (k), a strong enhancement of resonant dynamics occurs.

3. Zero field step resonances (ZFS) for $k > N$. From Figs. 3, 4 and 6, it is evident that we can also find ZFS resonances at order $k > N$. In conventional systems at larger voltages, ZFS resonances are never present [47]. A direct observation of phase dynamics shows that it is similar to standing wave configurations. In other terms, localized semifluxons generate a magnetic field which influences the ZFS dynamics making it more similar to a FS dynamics in conventional systems, which is in between the pure solitonic dynamics and Kulik standing wave approach. Indeed, ZFS structures exist also for $k \gg N$ [48], but they are faint and of small amplitude. In this case, the phase dynamics is found to be identical to a cavity mode pattern, so these structures correspond to Fiske step in Kulik theory.

Though highest order steps are easily visible in the global 2d plot in Figs. 3 and 4, the lowest order step are often hidden by the critical current pattern. When possible, we report the lowest k resonance pattern which is stable, over the chosen magnetic field range, in the bottom inset of Figs. 3 and 4 [49].

3.3 Resonances dynamics

In the following subsections, we describe the inner phase dynamics for some of the lowest resonances and for the lowest values of N. All subsequent outcomes are consistent with the intuitive idea that in the presence of semifluxons, the behavior of the unconventional junction is "shifted" by an half-flux quantum. On the other hand, the presence of localized magnetic field moments, due to semifluxons, favors the presence of e.m. cavity modes because the local field of semifluxons behaves as an external field. In the presence of faceting, cavity modes can occur also at magnetic fields below the Tinkham field $\eta = 2$, especially for high values of k when the junction is unable to support solitonic propagation. This observation explains the abovementioned presence of ZFS for high values of k, which is not found in conventional junctions.
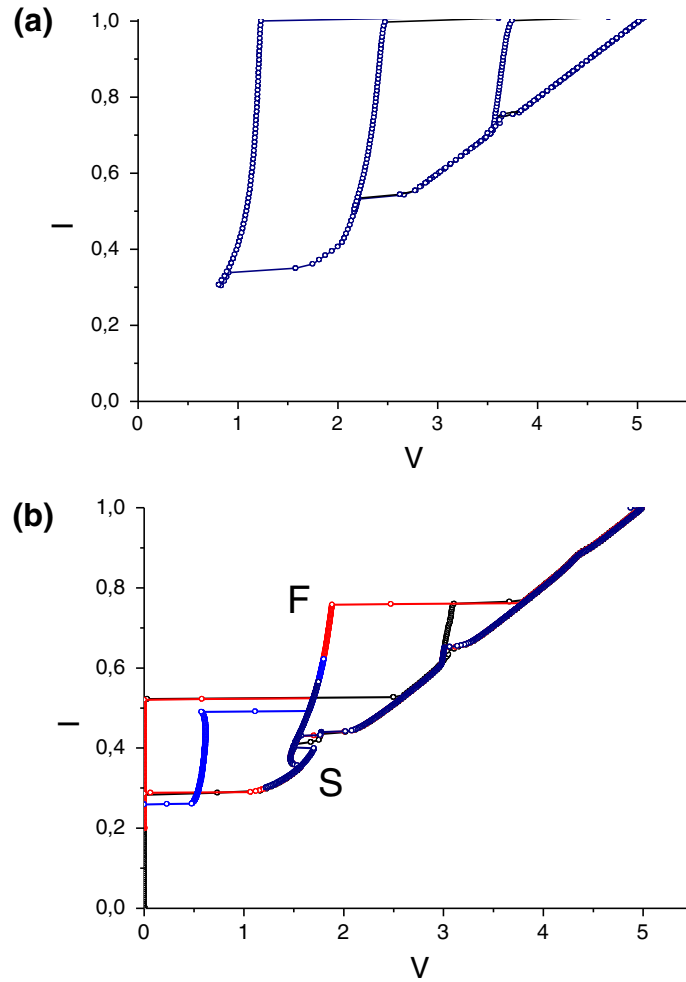
Fig. 7 I–V characteristic for a conventional (**a**) and a $N = 2$ facets (**b**) junction with $l = 5$, $\alpha = 0.2$ and zero magnetic field η

3.3.1 Zero field resonances for $N = 2$

The first three zero field resonances (ZFS's) are reported for a conventional and a two facets junction ($N = 2$) with $l = 5$ and $\alpha = 0.2$, respectively, in Fig. 7a, b. Only three resonances appear for these values of l and of the dissipation. The resonance voltage position of the two-faceted junction is lower, for it actually corresponds to odd values of k. Indeed, we find $V_3 \simeq 1.26$ and $V_4 \simeq 2.49$ for the first two resonances in Fig. 7a, and $V_1 \simeq 0.63$ and $V_2 \simeq 1.85$ in Fig. 7b. Thus, in faceted junction, the zero field resonances appear at the Fiske step odd position ZFSk/2.

In conventional hysteretical junction, the ZFS are large well-defined resonances corresponding to free motion of one or more fluxons back and forth in the junction. The largest resonance is ZFS1 ($k = 2$) which is about 70% of critical current in this simulation. In the faceted junction, the largest step of about 45% of the critical current is found for order $k = 3$ (ZFS3/2). This step in Fig. 7b appears clearly splitted in two branches each corresponding to different dynamical states: S (Standing) bottom branch and F (Fluxon) top branch.

On the ZFS1/2 ($k = 1$), the dynamics reduces to simple flips of central semifluxon making phase advance of 2π for period, by emission of fluxons–antifluxons which are annihilated at the boundary. Next, orders ($k > 1$) for (F) top branches can be viewed as the superposition of this flip dynamics with fluxons–antifluxons annihilated at boundary with propagating fluxons reflected at boundary.

In Fig. 8a, a simulation of ZFS3/2 dynamics is shown by a 2d plot of the voltage $\varphi_t(x, t)$ as function of x and t. The dynamics at $\gamma = 0.73$ (F branch) is due to the propagation of a single fluxon going back and forth in the junction. At this order, ZFS do not exist in conventional junction ($N = 1$), so the observed dynamics
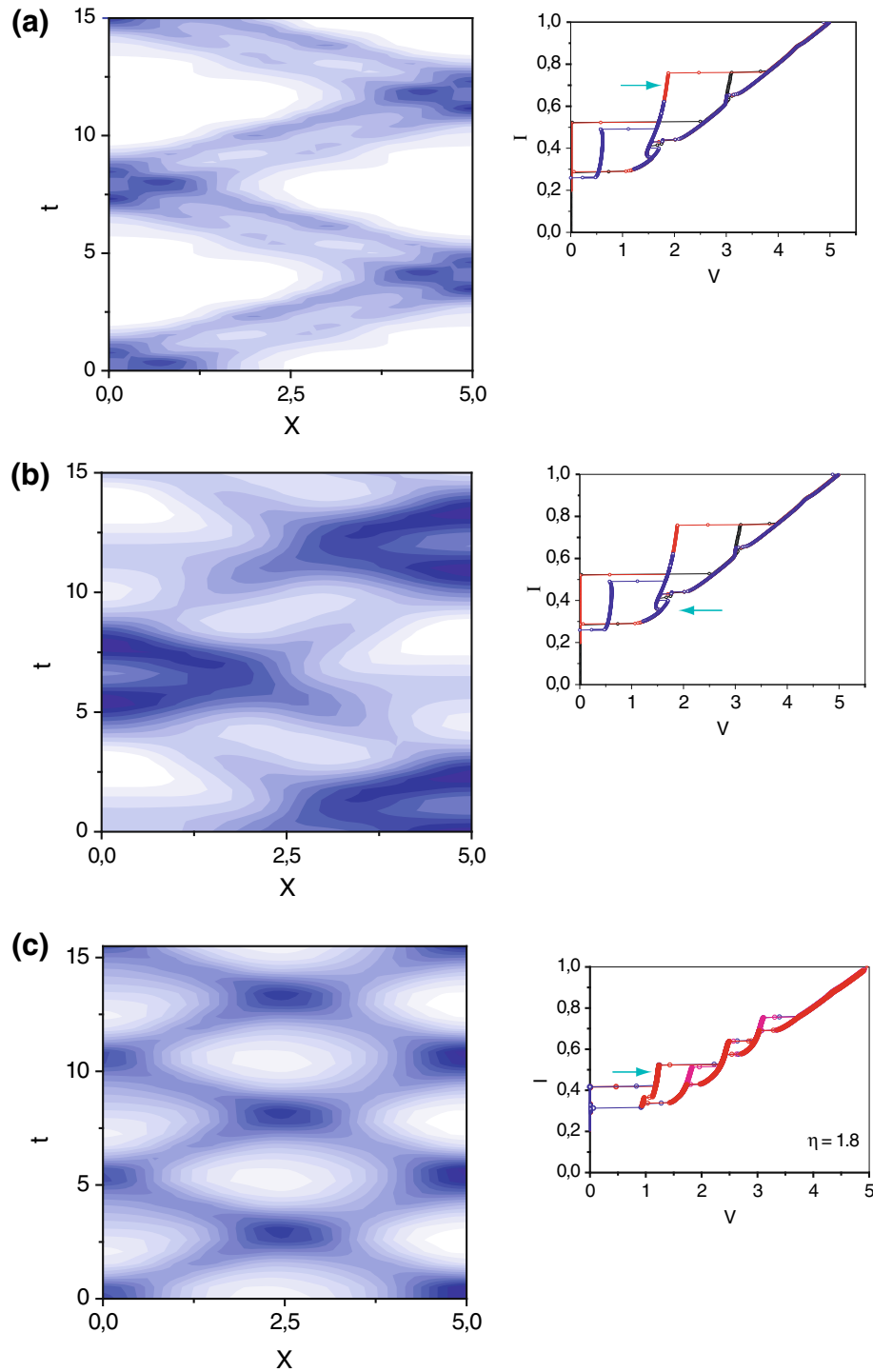
Fig. 8 Simulated resonant dynamics for $N = 2$, $l = 5$ and $\alpha = 0.2$. The 2d plot shows the voltage $V(x, t) = \varphi_t(x, t)$ as a function of space, x, and time, t, in the junction, *darker gray* corresponds to highest voltages; in all cases, the *insets* with I–V characteristics to the *right show with an arrow* the point on step where the simulation was made: **a** $k = 3$ resonance (ZFS3/2) higher part at $\gamma = 0.73$; **b** $k = 3$ resonance (ZFS3/2) lower part at $\gamma = 043$; **c** $k = 2$ resonance (FS2) at $\gamma = 0.49$ and $\eta = 1.8$

should be considered as a new dynamical solution, which involves, in addition to fluxon dynamics, successive flips of the semifluxon in the center of the junction [23]. The solution is similar to the conventional ZFS fluxon propagation, which carries a 4π increase in the phase, and two semifluxon flips per period, which contribute with an additional rotation of 2π to obtain a 6π increase of the phase.

A similar dynamics is also observed on the step of the order $k = 5$, the so-called ZFS5/2. The required phase sweep of 10π is due to the addition of a propagating fluxon–antifluxon pair, which gives an 8π plus another 2π from two semifluxon flips per period. The 2π rotation is triggered by the pair virtual annihilation at the center which occurs twice per period.

In Fig. 8b, we report again the dynamics as 2d plot of $\varphi_t(x, t)$ on the $k = 3$ resonance but at $\gamma = 0.43$ over the S branch of the I–V curve (see Fig. 7b). Alternating between two boundaries, the phase difference increases of about $3\pi \sim 9$ for each semiperiod ($k = 3$). Fluxons again propagate from and to the boundaries, but the semifluxon acts as a reflecting boundary for the fluxon at the center. A flip of semifluxon occurs for each reflection, so in the complete period we again have an increase of $4\pi + 2\pi$. Here, the dynamics is more static, i.e., more similar to a "standing" wave, because the bias current is too low to drive the fluxon through the semifluxon singularity in the middle of junction. The dynamics is similar to ZFS1/2, but the entrance of fluxons–antifluxons in the junction occurs at a rate twice faster than the $k = 1$ resonance. A similar mechanism is described in [25], but without a truly resonant behavior, for the higher dissipation produces a random input of fluxons. Here, the dynamics is clearly resonant, and the propagation of fluxon strongly interacts with the localized semifluxon. The coexistence of different resonant dynamics in the same resonance has been previously observed in the presence of a magnetic field [31], and here for the first time, we observe it at zero magnetic field. In simulations, we have found the two separated branches for any length between $l = 1$ and $l = 8$ and for dissipation below $\alpha \sim 0.3$.

3.3.2 Resonances at finite magnetic field for $N = 2$

The magnetic field patterns of the $k = 1$ and $k = 3$ (F branch) resonances are given in the bottom inset of Fig. 3 as sharp peaks [48]. The $k = 3$ (F branch) resonance is also visible behind the critical current pattern as a peak in the main 2d plot. The behavior of these resonances is compatible with a "pure" bidirectional solitonic dynamics surviving for very low fields as in conventional systems [31]. In fact, for higher magnetic fields $|\eta| > 0.6$, only small standing wave Fiske steps remain. The structure of numerically simulated patterns is similar to the analytical approach [36,48], but the lobe amplitudes are different due to nonlinear effects in Eq. (1), which are not included in the linear cavity modes theory of the Kulik approach for long junctions.

The $k = 3$ (F branch) resonance (red circles) merges with the $k = 3$ (S branch) resonance (green circles) at a low field $|\eta| \simeq 0.4$. We observe that the $k = 3$ (S branch) pattern shows a minimum at zero field. The two maxima occur at $|\eta| \sim 1.3$. The presence of the maxima can be related to the magnetic field generated by the semifluxon in the middle of the junction, similar to what happens in the case of ZFS1 ($k = 2$) for $N = 2$, as described below.

In Fig. 8c, the dynamics for the same junction is shown as a 2d plot of $V(x, t)$ in presence of a magnetic field $\eta = 1.8$. We observe an apparently symmetric solution more similar to a ZFS where two fluxons travel back and forth in the junction. Anyway, the total increase of the phase along a period is 4π, so the resonance is actually in ZFS1 position.

This is different from conventional junction where a one-directional fluxon motion is present due to the boundary magnetic field. Indeed, the presence of semifluxons in magnetic field could determine situations with zero or very low field gradient. In these conditions, fluxons can travel freely as in the ZFS dynamics and can be reflected at boundary rather than annihilated as in conventional one-directional FS dynamics. The semifluxon provides an alternating magnetic field, and the summing of its field to the external field is responsible for a "field gradient cancellation".

To cancel the field gradient, the semifluxons should amount to the equivalent field magnetic moment. A rough analysis can be made by representing the boundary magnetic field as $(\downarrow) \cdots (\uparrow)$. The arrows here do not represent necessarily a half flux quantum $\Phi_0/2$, for the magnetic field is variable. In between the boundaries, we can add localized semifluxons $\uparrow$ or $\downarrow$ and propagating fluxons $\Uparrow$ (anti-fluxons $\Downarrow$). These last by convention propagate to the left (right) due to bias current drive and are repelled by equal polarity moments and attracted by opposite polarity moments. In a resistive state dynamics, an underlying phase uniform velocity can add to localized moments. All this sum up in the junction resulting in a complex dynamics.

In conventional junctions, the FS dynamics is represented by asymmetric propagation of fluxon $\Uparrow$ to the left, and this occurs because the bias current adds to the external field making possible the penetration of fluxon toward the right end. Then, the bias current will be responsible to drive it toward the left end. Conventional dynamics is represented by $(\downarrow) \Uparrow (\uparrow)$. The $\Uparrow$ fluxon is annihilated and not reflected at the left boundary because reflection is inhibited by low values of local field generated by the different signs of bias current and the external field.

In the $N = 2$ faceted junction, the dynamics can be represented at a given time by $(\downarrow)$ $\Downarrow\uparrow\Uparrow$ $(\uparrow)$, and the $\Uparrow$ fluxon propagates to the left (almost) freely, because the semifluxon and the field at the right boundary have the same polarity (gradient cancels). At the same time, a back-reflected anti-fluxon $\Downarrow$ propagates to the right in the left facet. After the semifluxon flips and fluxons are reflected at the facets boundary, the configuration changes in $(\downarrow)$ $\Uparrow\downarrow\Downarrow$ $(\uparrow)$; the $\Uparrow$ continue (almost) freely to the left and a back-reflected $\Downarrow$ is created in the right facet. In the Fig. 8c, the propagation of fluxon $\Uparrow$ appears to be continue through the facet boundary and a well-defined voltage peak. On the contrary, the $\Downarrow$ anti-fluxon shows a less-defined voltage peak. The phase increase remains limited to 4π just because $\Downarrow$ annihilate before to reach the boundary.

This is confirmed by a similar dynamics encountered on the lower part of the $k = 2$ resonance $0.31 < \gamma < 0.37$. This dynamics is incoherent, i.e., back-reflected anti-fluxons from the unfavorable left boundary sometimes did not occur and the dynamics is sometimes one-directional as in conventional FS.

3.3.3 Resonances for $N > 2$

For N odd, e.g., $N = 3$ (Fig. 4), the opposite happens: There are no ZFSs for odd k. A deep minimum is present in these cases (cfr. Fig. 4 lower inset), and it is likely that there is no free fluxon propagation. For even k, a maximum of the pattern is found as in conventional systems [50].

When the number of facets increases to $N = 3$, we find a dynamics which is similar to the previous case. For example, we consider the step of $k = 2$ order (ZFS1), whose dynamics represented a 2d plot of $V(x, t)$, is shown in Fig. 9a. The dynamics can be schematized as: (1) fluxons propagate from boundary; (2) a large phase oscillation (breather) is generated in the central facet; (3) finally, the two fluxons emerge and propagate toward the boundary. A direct analysis reveals two semifluxons, which are oscillating from $\uparrow\downarrow$ to $\downarrow\uparrow$ as it is shown in the lower inset of Fig. 9a. This process gives a 4π increase of the phase per period, exactly what is needed for the $k = 2$ resonance. In terms of magnetization, the original configuration can be represented as $\Downarrow\uparrow\downarrow\Uparrow$, which turns into $\downarrow$ $(\Downarrow\Uparrow)$ $\uparrow$ and $\downarrow$ $(\Uparrow\Downarrow)$ $\uparrow$, where the parenthesis indicates the breather formed by fluxon–antifluxon pair in the central facet and ends after the semifluxon polarity is restored with $\Uparrow\uparrow\downarrow\Downarrow$.

The most peculiar solution is found in presence of a magnetic field. The resonance $k = 2$ shows a symmetric fluxon dynamics practically similar to the ZFS1 dynamics in conventional junctions (see Fig. 9b). This solution is fully explained by "field gradient cancellation." Semifluxons are now adapting to the external field to cancel the field gradient in order to permit a symmetric propagation of fluxon for such large magnetic field $\eta = 1.8$. We have, for example: $(\downarrow)$ $\Downarrow\downarrow\uparrow$ $(\uparrow)$ where $\Downarrow$ represents the propagating anti-fluxon going toward the right. In the next facet, the configuration changes in: $(\downarrow)$ $\uparrow\Downarrow\uparrow$ $(\uparrow)$. Finally, in the last facet: $(\downarrow)$ $\downarrow\uparrow\Downarrow$ $(\uparrow)$ with again a gradient cancelation given by the $\uparrow$ semifluxon. This dynamics is not observed for $N = 2$ (Fig. 8c) because in that case symmetry requires two fluxons interacting with a single semifluxon. Therefore, in that case, the back-reflected anti-fluxon $\Downarrow$ is annihilated because it is unable to complete the back and forth cycle.

As in the $N = 2$ case, the phase dynamics on the other resonances at zero field is similar. The dynamics on the large $k = 5$ resonance in presence of external field $\eta = 1.8$ is shown in Fig. 9c. These solutions resemble cavity modes because the $l = 5$ junction is too short to "accommodate a complex dynamics" and propagation of fluxons is practically not observed for higher orders. The voltage (or magnetic field) rather presents an oscillating peak in which fluxon and semifluxon modes are mixed.

3.4 Effect of temperature

The effect of the temperature on resonances is reported in Fig. 10 in zero magnetic field, which represents the thermodynamical maximum amplitude of resonances in the phase space (η, T) for a junction with $I_0 = 1\,\mu A$. As it is shown in (a) and (b) for $N = 2$ and $N = 3$ facets, respectively, the amplitude of F-resonances rapidly decrease in temperature so that at about $T \simeq 1.8$ K all F-resonances completely disappear. The $k = 1$ resonance for $N = 2$ disappears at $T = 1.2$ K. On the other hand, traces of faint S-resonances remain at very small steps until $T = 3.0$ K and beyond. This behavior is consistent with observed small stability range of ZFS and in general of fluxon propagation in magnetic field; indeed, when a magnetic field is applied in conventional systems, amplitude of the ZFS is strongly reduced and goes to zero well before Tinkham field. This behavior is observed here for all F-resonances, which disappear for very small magnetic fields $\eta \simeq 0.2$.
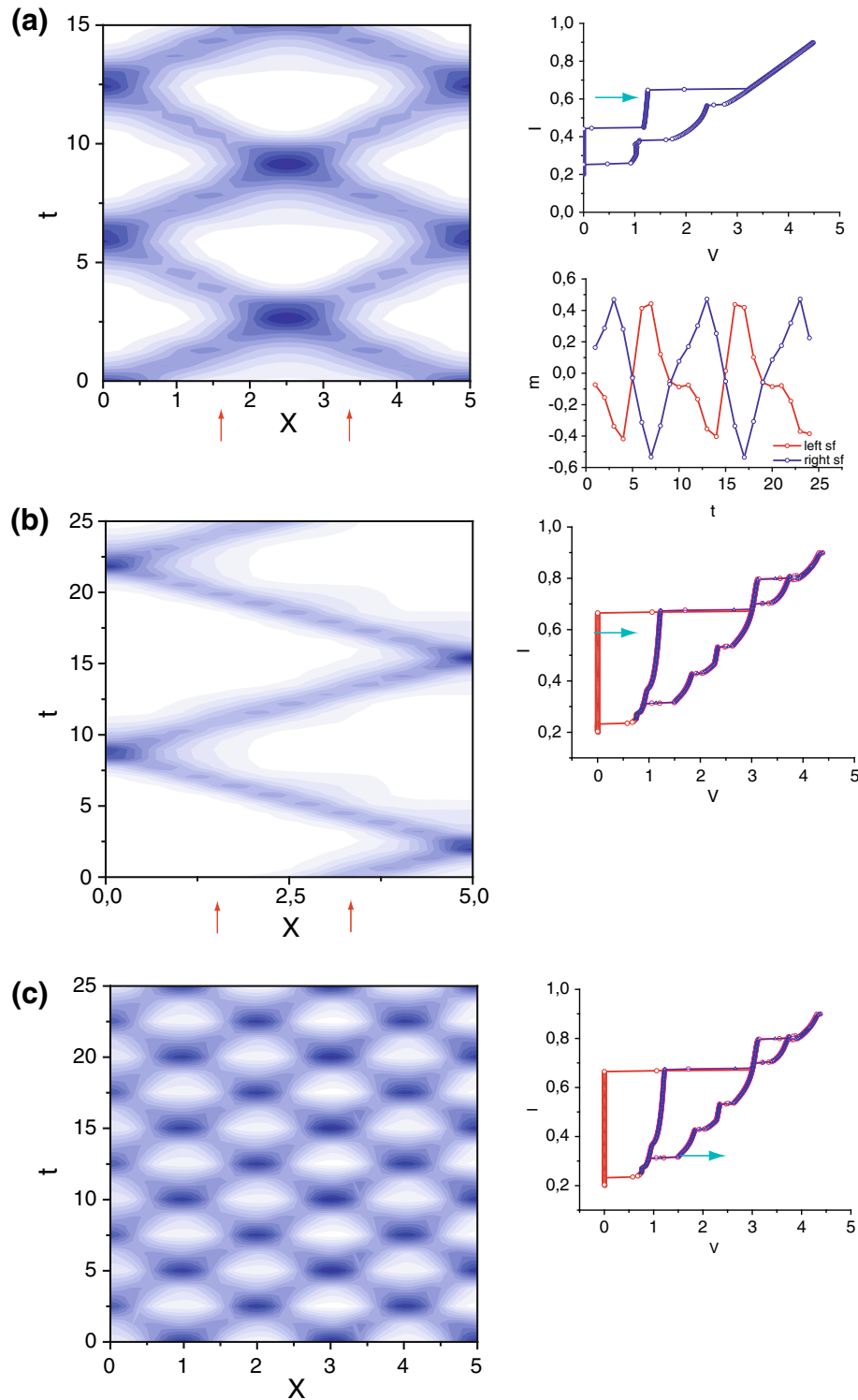
Fig. 9 Simulated resonant dynamics for $N = 3l = 5$ and $\alpha = 0.2$. The 2d plot shows the voltage $V(x, t) = \varphi_t(x, t)$ as function of space and time in the junction, *darker gray* corresponds to highest voltages; in all cases, the *insets* with the I–V characteristics at *right show with an arrow* the point on step where simulation was made: **a** $k = 2$ resonance (ZFS1) at $\gamma = 0.6$; **b** $k = 2$ resonance (FS2) at $\gamma = 0.6$ and $\eta = 1.8$; **c** $k = 5$ resonance (FS5) at $\gamma = 0.75$ and $\eta = 1.8$. The *lower inset* near **a** shows the local field at semifluxon positions for the same times of 2d plot
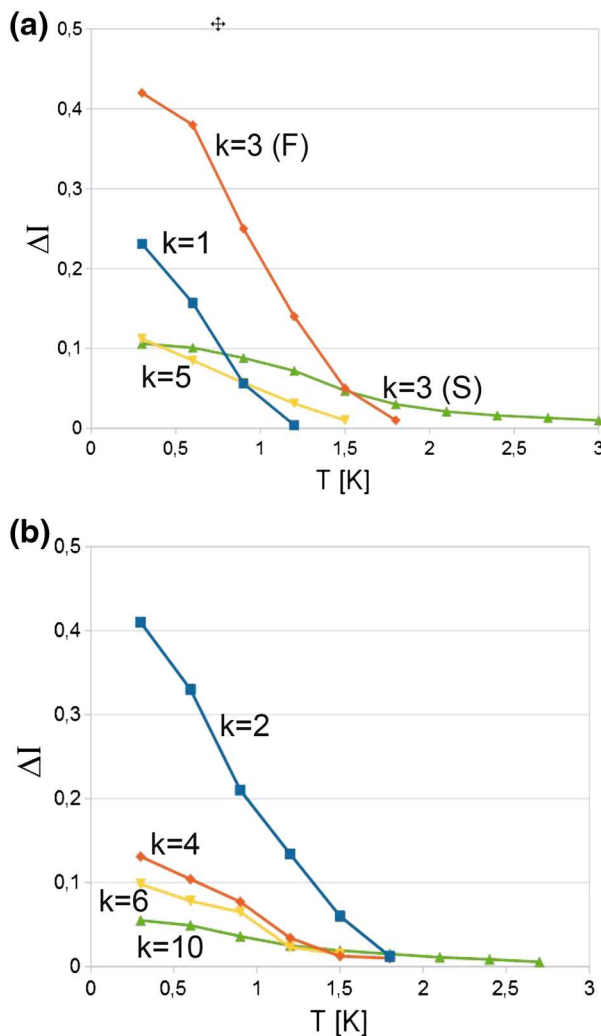
Fig. 10 Effect of temperature on the resonance amplitude ΔI (normalized to critical current) for T varying from 0.3 to 3.0 K for: **a** $N = 2$ facets junction with $l = 5$, $\alpha = 0.2$ and zero magnetic field η; **b** $N = 3$ facets junction with $l = 5$, $\alpha = 0.2$ and zero magnetic field η. Resonances are indicated by index k on all plots

4 Measurements on grain boundary YBCO Josephson junctions

Until now, Josephson junctions have been successfully applied to voltage standard devices [51], SQUID magnetic sensors [52] and integrated microwave detectors and generators [53,54]. The unconventional d-wave order parameter symmetry (OPS) still remains one of the unique superconducting features of HTS [55], with significant implications both for the study of fundamental issues and for innovative applications [56]. After the first pioneering experiments [57,58], all the following ones employing junctions basically confirmed the prevalence of a d-wave OPS and envisaged some novel and intriguing physics of the Josephson systems [27,28].

For grain boundary junctions, the phenomenology is deeply influenced by the type of microstructure, which through the presence of different kinds of impurities and imperfections, including the meandering of the grain boundary line, may also mask an intrinsic d-wave effects [27,28]. Even if not ideal, there are some examples of high-quality HTS junctions and films, which on one hand allows the realization of working devices such as SQUIDs [28] and, on the other hand, have been used to prove macroscopic quantum effects [44,45,59–61] and fast femtosecond phenomena on bilayers [62].

Here, we point our attention, in particular, to the variety of resonant modes, determined by both the low dissipation and a d-wave order parameter in presence of a faceted grain boundary interface. Faceting can be
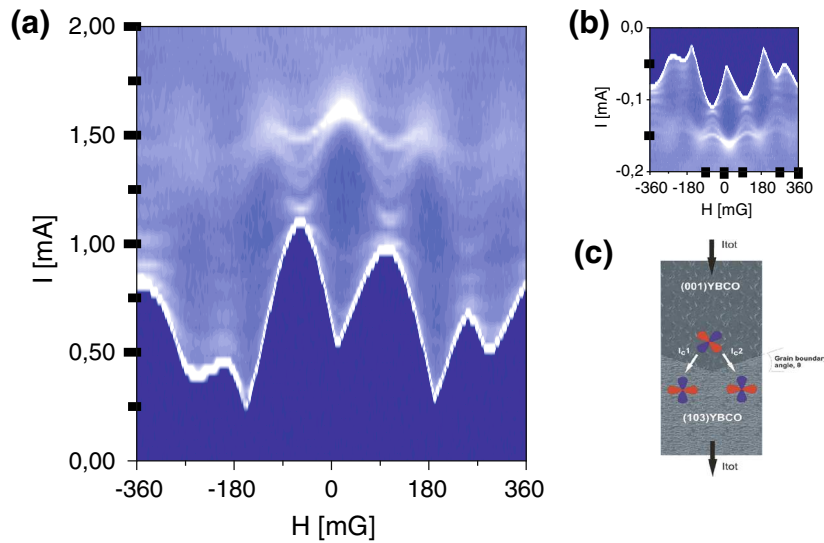
Fig. 11 2D plot of experimental dV/dI as function of current and magnetic field for the "corner" YBa$_2$Cu$_3$O$_{7-x}$ biepitaxial junction sketched in the *top inset*; the junction will have $\alpha \sim 1$ and $l \sim 6$. The measurements temperature was $T = 0.3$ K. Among steps recognizable above the critical current pattern are some external LC resonances due to kinetic inductance and a well-marked large ZFS which behavior is affine to Eck singularities in ordinary junctions. In the *lower inset*, we report the negative bias current pattern to check point symmetry against potential trapped flux

"artificial," realized with an opportune shape of the seed layer, or intrinsic, due to microfaceting along the junction GB.

All samples were prepared by the bi-epitaxial technique described in detail in [26,29,63,64]. Briefly, a 30 nm-thick seed layer of CeO$_2$ (CeO) was deposited on a (110) oriented STO substrate by pulsed laser deposition (PLD). The seed layer was patterned using direct e-beam lithography and Ar$^+$ ion etching through an amorphous carbon, (*a*-carbon), mask. The residual a-carbon was removed by low-power oxygen plasma etching, and a 100 nm-thick layer of YBCO was deposited by PLD. The YBCO grows following the (103) orientation on the substrate and the (001) one on the seed layer. A GB is thereby created where the orientations meet. Additionally, the (001) grains are rotated of 45° the *c*-axis with respect to the (103) ones. This additional rotation reflects on the order parameter. Gold contact pads are made in another lithography step, and finally, the YBCO is patterned using direct e-beam lithography and Ar$^+$ ion etching through an *a*-carbon mask. Sketches of the samples are shown in the SEM pictures reported in the insets of Figs. 11 and 12. In Fig. 11, an artificial two facets corner junction is seen with a GB angle of $\theta = 15°$. One can clearly identify the two facets of the junction. Both facets have a length of 5 µm each, so total physical length is $L = 10$ µm. The right facet has an intrinsic phase shift of π, which is induced by the transport across the interface from $a+$ to $a-$ lobe of the order parameter. Instead, the left facet has zero intrinsic phase shift because the order parameters in the two electrodes have the same sign in direction normal to the interface. In Fig. 12, a submicron single facet junction with $L = 0.8$ µm and a GB angle of $\theta = 50°$ is reported.

The measurements have been performed in an Oxford Heliox VL 3He refrigerator. The cryostat is magnetically shielded. The current–voltage characteristics of the sample have been recorded in a four-point configuration. An external magnetic field (parallel to the sample surface normal) is applied to the sample by feeding a dc current through a superconducting coil surrounding the sample.

The experimental complete magnetic field pattern of biepitaxial corner junction is reported in Fig. 11 a 2D plot of dynamical resistance R_d. The data appear very similar to simulated $N = 2$ facets reported in Fig. 3. From the critical current of $I_0 \sim 120$ µA, a Josephson penetration depth λ_J of about 2.1 µm is found. The normalized length is $l \simeq 4.8$ [65].

Behind the critical current pattern, several resonances are observed in R_d plot. Small resonances at finite field, $H \sim 90$ and 250 mG, are likely due to junction coupling to a kinetic inductance LC-circuit [79]. These resonances appear at small voltages under 100 µV and are compatible with LC frequencies.

A well-marked resonance is present at zero field with a magnetic field pattern pretty close to the numerical results of Fig. 3. Due to high value of the product $\alpha l \sim 5$ (dissipation $\alpha \sim 1$ for this junction), the resonance
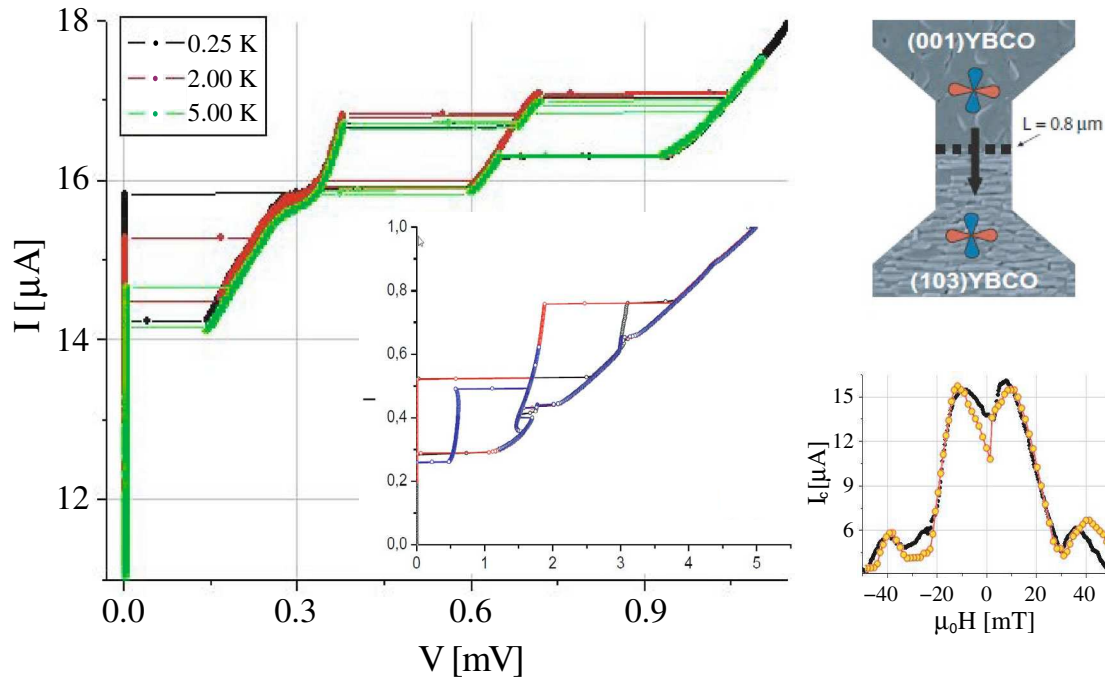
Fig. 12 Some I–V characteristics for a submicron (0.8 μm) in zero magnetic field $YBa_2Cu_3O_{7-x}$ biepitaxial junction sketched in the *top inset*. The junction estimated parameters are $\alpha \sim 0.4$ and $l \sim 3.8$. The measurement temperatures are reported in the legend. The experimental critical current magnetic field pattern is shown in the *lower inset* with *full black dots*. The simulated pattern (*red/yellow dots*) is obtained with an asymmetric faceting with $N = 2$, $\alpha = 0.4$ and $l = 5$ with facets length $a_1 = 2.7$ and $a_2 = 2.3$ (color figure online)

appears as a broad coalescence of magnetic field modes. The resonance extends over the voltage range 200–400 μV.

A submicron junction has been realized with a single facet, even if the presence of a random submicron faceting cannot be excluded. I–V characteristics from the submicron junction are reported in Fig. 12. Resonance in zero field is clearly visible implying that dissipation levels are below some threshold value and that comparing with numerically we can estimate of the order of $\alpha \sim 0.4$. Moreover, the resonance structure is very similar to Fig. 7b at zero field: In particular, lowest resonances appear splitted in a top (F) and a lower branch (S) as described in Sect. 3.3.1. Higher dissipation will make resonances more stable in temperature, but much more smaller than the simulated ones at $\alpha = 0.25$ (at $T = 5$ K resonance widths are less than 5 % of critical current). The hysteresis loop between (F) and (S) branches is not visible at this dissipation level.

The critical current magnetic field pattern, shown in the lower right corner of Fig. 12 (black dots), is compatible with an asymmetric $N = 2$ facets. A central depression of critical current is suggestive of possible presence of a "flip" lines in the middle. We show also (red/yellow dots) a simulated pattern obtained with only two asymmetric facets, $a_1 = 2.7$ and $a_2 = 2.3$ for a total length of $l = 5$ and $\alpha = 0.4$. The simulated pattern is very close to the experimental one reproducing its main features.

Here, the measurement at $T = 0.3$ K gives $I_c = 15.9$ μA. In presence of semifluxons, the total Josephson current is reduced by a factor depending on numbers of facets in the junction, and this could vary between 70 (two facets) and 15 % (many random facets). Therefore, an estimated Josephson current ranging from $I_0 \simeq 22.7$ to 106 μA can be estimated with a Josephson length of $\lambda_J \sim 210$–454 nm (for a London length of about $\lambda_L \sim 900$ nm, which is compatible with a 50° junction [29]). These values are consistent with a maximum value of $l = 3.8$ and therefore not far from the parameters used in the simulations of the pattern and I–V curves of Fig. 12. The ∼25 % difference in normalized length can be attributed to following factors: (1) lacking of an exact knowledge of the current distributions in the junction; (2) errors in the exact value of London length; (3) the exact 3D structure of the barrier is not known, and therefore, we do not have a reliable estimate of "effective" junction width w. We believe that recent advances in the fabrication and understanding of GB JJs will provide additional test benches also for resonant modes for these types of d-wave devices. On one hand, there is the possibility to change the capacity and the dissipation of the GB junctions by replacing

the STO with a LSAT substrate [59,60]. On the other hand, the possibilities for a further shrinking of the size of the junction in the deep submicron regime [26,61,79] seem more concrete, also pushed by the capability of realizing high-quality YBCO nanowires [66–68].

Finally, the faceted Sine–Gordon system considered here could have possible implications and use in the description of new devices called nanomechanical transistors [69]. Their working principle is based on the coupling of mechanical vibration of a nanopillar or a nanograin within a gap between two electrodes. The mechanical motion permits to transfer electrical charge between the two electrodes because of a quantum tunneling effect, and complex electro-mechanical phenomena arise [70,71]. Sine–Gordon model could be useful in the description of the system.

5 Conclusion

We have numerically simulated PSG equation representative of long faceted Josephson junctions and calculated the pattern of both the critical current and of the lower-order resonances appearing in the I–V characteristics. Some of these resonances show a nontrivial dynamics due to the interaction of propagating fluxons with localized semifluxons. Numerical outcomes have been compared with experimental data on YBCO biepitaxial JJs, prepared to have a low number of facets and relatively low dissipation levels when compared with all HTS JJs. The main results coming out from our analysis can be resumed as follows.

We found critical current patterns composed by different overlapping lobes due to the presence of different stable semifluxon distributions along the junction. Therefore, in the case of intermediate length junction, "flip" lines can separate different static configurations. The flip lines correspond to the flip of some semifluxons driving the junction in a different static configuration. This "dynamics" between static configurations, previously analyzed also in the work of Goldobin et al. [18], can also drive the junction to the resistive state when the dissipation is low. In short junctions, these configurations can be also identified by Eq. (2) (see Refs. [19,20]), but this model does not give information on the stability of semifluxons configuration, and it is not possible to predict the pattern and the position of flip lines. The actual pattern will depend on the initial configuration of the semifluxons in the junction.

Resonance patterns present a rich phenomenology with interplay between propagating and cavity modes solutions. The exact boundary between the two types of dynamics is not exactly defined, mainly because the Tinkham field is sometimes exceeded by the field generated by the semifluxons. Therefore, cavity modes can exist also at very low or zero magnetic field.

Thus, standing wave patterns (Fiske step) also appear at zero field for the lowest orders, and their dynamics is found in competition with zero field fluxon propagation [23,48]. In intermediate length junctions $l \sim 5$, the interaction between fluxons and semifluxons is observed also at relatively low dissipation ($\alpha < 0.2$). This interaction has two main consequences: (1) fluxons can be absorbed and/or reflected by semifluxons giving rise to a shift in the phase increase per period, which is the dynamical signature of π-shift, and this implies the presence of ZFS for odd values of k; (2) a semifluxon can add its field to the external field (or to other semifluxons) decreasing the field gradient, which is responsible for FS asymmetric dynamics. As a consequence, an almost symmetric phase dynamics can take place at finite magnetic field.

Nonlinear effects in the reflection from semifluxons can be compared with other nonlinear model reflections from a stress region [72–74]. Varying continuously the amplitude of phase difference generates a magnetic interface between two facets in which energy is proportional to square gradient of phase, i.e., the local magnetic field, which is similar to higher gradient theories in continuous mechanics [75]. On the other hand, there are many problems in which nonlinear electrical transmission lines coupled between them [76] or to mechanical elements [77,78] show an analog complex behavior.

Measurements on YBCO biepitaxial junction show many of the predicted features emerging from the simulations. In the case of artificial "corner" biepitaxial junctions (Fig. 11), high dissipation $\alpha \sim 1$ resonances appear as a large step, (all smaller resonances are due to LC coupling [79]). Several resonances in the experiments appear at both zero and finite magnetic field in submicron low dissipation "single" facet biepitaxial junctions (Fig. 12). Intrinsic submicron faceting can explain both the structure of resonances and the critical current magnetic field pattern.

References

1. Luongo, A., Zulli, D.: Dynamic instability of inclined cables under combined wind flow and support motion. Nonlinear Dyn. **67**(1), 71–87 (2011)
2. Luongo, A., Zulli, D., Piccardo, G.: Analytical and numerical approaches to nonlinear galloping of internally-resonant suspended cables. J. Sound Vib. **315**(3), 375–393 (2008)
3. Luongo, A., Zulli, D.: Dynamic analysis of externally excited NES-controlled systems via a mixed Multiple Scale/Harmonic Balance algorithm. Nonlinear Dyn. **70**(3), 2049–2061 (2012)
4. McLaughlin, D.W., Scott, A.C.: Fluxon interactions. Appl. Phys. Lett. **30**, 545 (1977)
5. Filatrella, G., Parmentier, R.D., Rotoli, G.: Phase locking of fluxons oscillations in long Josephson junctions with surface losses. Phys. Lett. A **148**, 122 (1990)
6. Filatrella, G., Rotoli, G., Salerno, M.: Suppression of chaos in Sine–Gordon system. Phys. Lett. A **178**, 81 (1993)
7. Ustinov, A.V., Cirillo, M., Larsen, B.H., Oboznov, V.A., Carelli, P., Rotoli, G.: Experimental and numerical study of dynamic regimes in a discrete sine–Gordon lattice. Phys. Rev. B **51**, 3081 (1995)
8. Petraglia, A., Filatrella, G., Rotoli, G.: Self-field effects in Josephson junctions arrays. Phys. Rev. B **53**, 2732 (1996)
9. De Leo, C., Rotoli, G., Nielsen, A., Barbara, P., Lobb, C.: Mutual inductance route to paramagnetic Meissner effect in 2D arrays of Josephson junctions. Phys. Rev. B **64**, 144518 (2001)
10. Filatrella, G., Rotoli, G., Grombech-Jensen, N., Pedersen, N.F., Parmentier, R.D.: Model studies of long Josephson junction arrays coupled to high-Q resonator. J. Appl. Phys. **72**, 3179 (1992)
11. Rotoli, G., De Leo, C., Ghigo, G., Gozzelino, L., Camerlingo, C.: Josephson junction network as a tool to simulate intergrain superconducting channels in YBCO films. Int. J. Phys. B **14**, 3068 (2001)
12. De Leo, C., Rotoli, G.: Magnetization of multiply connected superconductors with and without π-junctions loops. Supercond. Sci. Technol. **15**, 1716 (2002)
13. Pignataro, M., Luongo, A.: Asymmetric interactive buckling of thin-walled columns with initial imperfections. Thin-Walled Struct. **5**(5), 365–382 (1987)
14. Luongo, A.: Mode localization in dynamics and buckling of linear imperfect continuous structures. Nonlinear Dyn. **25**(1–3), 133–156 (2001)
15. Belyakov, A.O., Seyranian, A.P., Luongo, A.: Dynamics of the pendulum with periodically varying length. Physica D Nonlinear Phenom. **238**(16), 1589–1597 (2009)
16. Kirtley, J.R., Moler, K.A., Scalapino, D.J.: Spontaneous flux and magnetic interference patterns in 0-π. Josephson junctions. Phys. Rev. B **56**, 886 (1997)
17. Rotoli, G.: Induced paramagnetic states by localized π-loops in grain boundaries. Phys. Rev. B **68**, 052505 (2003)
18. Goldobin, E., Koelle, D., Kleiner, R.: Ground states and bias-current-induced rearrangement of semifluxons in 0-π long Josephson junctions. Phys. Rev. B **67**, 224515 (2003)
19. Smilde, H.J.H., Ariando, B., Blank, D.H.A., Gerritsma, G.J., Hilgenkamp, H., Rogalla, H.: d-waveinduced Josephson current counterflow in YBa2Cu3O7/Nb zigzag junctions. Phys. Rev. Lett. **88**, 057004 (2002)
20. Hilgenkamp, H., Ariando, H.J.H.S., Blank, D.H.A., Rijnders, G., Rogalla, H., Kirtley, J.R., Tsuei, C.C.: Ordering and manipulation of the magnetic moments in large-scale superconducting π-loop arrays. Nature **422**, 50 (2003)
21. Goldobin, E., Stefanakis, N., Koelle, D., Kleiner, R.: Fluxon-semifluxon interaction in an annular long Josephson 0-π junction. Phys. Rev. B **70**, 094520 (2004)
22. Rotoli, G.: Unconventional Josephson junction arrays for qubit devices. IEEE Trans. Supercond. **15**, 852 (2005)
23. Stefanakis, N.: Resonant flux motion and I–V characteristics in frustrated Josephson junctions. Phys. Rev. B **66**, 214524 (2002)
24. Goldobin, E., Sterck, A., Gaber, T., Koelle, D., Kleiner, R.: Dynamics of semifluxons in Nb long Josephson 0-π junctions. Phys. Rev. Lett. **92**, 057005 (2004)
25. Lazarides, N.: Critical current and fluxon dynamics in overdamped 0-π Josephson junctions. Phys. Rev. B **69**, 212501 (2004)
26. Stornaiuolo, D., Rotoli, G., Cedergren, K., Born, D., Bauch, T., Lombardi, F., Tafuri, F.: Submicron YBaCuO biepitaxial Josephson junctions: d-wave effects and phase dynamics. J. Appl. Phys. **107**, 113901 (2010)
27. Tafuri, F., Kirtley, J.R.: Weak links in high critical temperature superconductors. Rep. Prog. Phys. **68**, 2573 (2005)
28. Hilgenkamp, H., Mannhart, J.: Grain boundaries in high-T$_c$ superconductors. Rev. Mod. Phys. **74**, 485 (2002)
29. Cedergren, K., Kirtley, J.R., Bauch, T., Rotoli, G., Troeman, A., Hilgenkamp, H., Tafuri, F., Lombardi, F.: Interplay between static and dynamic properties of semi-fluxons in YBaCuO Josephson junctions. Phys. Rev. Lett. **104**, 177003 (2010)
30. Salerno, M., Samuelsen, M.R., Filatrella, G., Pagano, S., Parmentier, R.D.: Microwave phase locking of Josephson-junction fluxon oscillators. Phys. Rev. B **41**, 6641 (1990)
31. Nappi, C., Lisitskiy, M.P., Rotoli, G., Cristiano, R., Barone, A.: New fluxon resonant mechanism in annular Josephson tunnel structures. Phys. Rev. Lett. **93**, 187001 (2004)
32. Fulton, T.A., Dynes, R.C.: Single vortex propagation in Josephson tunnel junctions. Solid State Commun. **12**, 57 (1973)
33. Kulik I.O., Zh. Eksp. Teor. Fiz., Theory of "steps" of voltage-current characteristic of the Josephson tunnel current, Pisma Red. **2**, 134 (1965) [JETP Lett. **2**, 84 (1965)].
34. Ernè, S.N., Ferrigno, A., Parmentier, R.D.: Fluxon propagation and Fiske steps in long Josephson tunnel junctions. Phys. Rev. B **27**, 5440 (1983)
35. Olsen, O.H., Samuelsen, M.R.: Fluxon propagation in long Josephson junctions with external magnetic field. J. Appl. Phys. **52**, 6247 (1981)
36. Cirillo, M., Gronbech-Jensen, N., Samuelsen, M., Salerno, M., Verona Rinati, G.: Fiske modes and Eck steps in long Josephson junctions: theory and experiments. Phys. Rev. B **58**, 12377 (1998)
37. Tinkham, M.: Introduction to Superconductivity. McGraw-Hill, New York (1996)
38. Pfeiffer, J., Kemmler, M., Koelle, D., Kleiner, R., Goldobin, E., Weides, M., Feofanov, A.K., Lisenfeld, J., Ustinov, A.V.: Static and dynamic properties of 0, π, and 0-π ferromagnetic Josephson tunnel junctions. Phys. Rev. B **77**, 214506 (2008)

39. The criterium is $\alpha l < \pi$, where best HTC junctions have $\alpha l \sim 4$. This implies an Eck step and/or Flux-Flow dynamics rather than a resonant dynamics
40. Barone, A., Paterno, G.: Physics and Applications of Josephson Effect. Wiley, New York (1982)
41. Goldobin, E., Vogel, K., Crasser, O., Walser, R., Schleich, W.P., Koelle, D., Kleiner, R.: Quantum tunneling of semifluxons in a 0-π-0 long Josephson junction. Phys. Rev. B **72**, 054527 (2005)
42. The length scaling is given by the simple formula $a_j = \bar{a}_j \sqrt{\frac{J_j}{\bar{J}_j}}$ where J_j is the critical current density in the model facet and $\bar{J}_j$ the critical current density in the original facet. Our assumption simply set $J_j = J_0 = 1$
43. Carcaterra, A., Akay, A.: Dissipation in a finite-size bath. Phys. Rev. E **84** (2011)
44. Bauch, T., Lombardi, F., Tafuri, F., Barone, A., Rotoli, G., Delsing, P., Cleason, T.: Macroscopic quantum tunneling in d-wave YBCO Josephson junctions. Phys. Rev. Lett. **94**, 087003 (2005)
45. Bauch, T., Lindstrom, T., Tafuri, F., Rotoli, G., Delsing, P., Cleason, T., Lombardi, F.: Quantum dynamics of a d-wave Josephson junction. Science **311**, 56 (2006)
46. Rotoli G.: *Magnetization states in annular Josephson junction π-arrays* in contributed book Research Signpost: New Developments in Josephson Junctions Research ISBN 978-81-7895-328-1, S. A. Sergeenkov ed., 2008
47. The presence of a ZFS of order k is a close consequence of the junction capacity to accommodate k propagating fluxons. As the spatial extent of a fluxon is roughly 1 in normalized units, when k is of the order of l fluxon dynamics become problematic and normally dissipation will inhibit solitonic dynamics even before this limit. Indeed in conventional junctions it is difficult to observe more than 3 ZFS for a junction normalized length $l \simeq 5$. Other effects came into play like "surface" dissipation which make the ZFS soon unstable (see S. Pagano, PhD thesis, The Technical University of Denmark 1986)
48. Nappi, C., Sarnelli, E., Adamo, M., Navacerrada, M.A.: Fiske modes in 0-π Josephson junctions. Phys. Rev. B **74**, 144504 (2006)
49. By "stable" here we mean that pattern is "accessible" by using the standard procedure to sweep bias current along the resonance. A low order step pattern could be difficult to be reached by sweeping the bias current just below the resonance because, at low voltage values, the phase can very easily return in the zero voltage state on the critical current. In some cases only by chance it is possible to reach these resonances quickly going up in bias current sweep. In nonlinear dynamics terms their "basin of attraction" is very small and could be bypassed by other larger attractors. Moreover, here we search this stability not just for one resonance, but for its full dependence on magnetic field
50. The complexity of the resonance pattern is increasing with N. The number of resonance pattern peaks at order $k = 1$ increases from 7 to 11 going from $N = 4$ to $N = 6$. The same happens for order $k = 2$, but in this case the increase is of just one peak per facet units, i.e., we go from 4 at $N = 2$ to 7 at $N = 5$. For the order $k = 3$ there is a similar increase of peak number, but the exact law is less clear because in some case, e.g., for $N = 5$ the large peaks may be cover the small peaks between them
51. Niemeyer, J.: Josephson voltage standards. In: Seeber, B. (ed.) Handbook of Applied Superconductivity, pp. 1813–1834. Institute of Physics Publishing, Bristol (1998)
52. Kleiner, R., Koelle, D., Ludwig, F., Clarke, J.: Superconducting quantum interference devices: state of the art and applications. Proc. IEEE **92**(10), 1534 (2004)
53. Zmuidzinas, J., Richards, P.L.: Superconducting detectors and mixers for millimeter and submillimeter astrophysics. Proc. IEEE **92**, 1597 (2004)
54. Barbara, P., Cawthorne, A.B., Shitov, S.V., Lobb, C.J.: Stimulated emission and amplification in Josephson junction arrays. Phys. Rev. Lett. **82**(9), 1963 (1999)
55. Tsuei, C.C., Kirtley, J.R.: Pairing symmetry in cuprate superconductors. Rev. Mod. Phys. **72**, 969 (2000)
56. Blatter, G., Geshkenbein, V.B., Ioffe, L.B.: Design aspects of superconducting-phase quantum bits. Phys. Rev. B **63**, 174511 (2001)
57. Tsuei, C.C., Kirtley, J.R., Chi, C.C., Yu-Jahnes, L.S., Gupta, A., Shaw, T., Sun, J.Z., Ketchen, M.B.: Pairing symmetry and flux quantization in a tricrystal superconducting ring of YBa2Cu3O7. Phys. Rev. Lett. **73**, 593–596 (1994)
58. van Harlingen, D.J.: Phase-sensitive tests of the symmetry of the pairing state in the high-temperature superconductors. Evidence for $d_{x^2-y^2}$ symmetry. Rev. Mod. Phys. **67**, 515 (1995)
59. Longobardi, L., Massarotti, D., Stornaiuolo, D., Galletti, L., Rotoli, G., Lombardi, F., Tafuri, F.: Direct transition from quantum escape to phase diffusion regime in YBaCuO biepitaxial Josephson Junctions. Phys. Rev. Lett. **109**, 050601 (2012)
60. Massarotti, D., Longobardi, L., Galletti, L., Stornaiuolo, D., Rotoli, G., Tafuri, F.: Macroscopic quantum tunneling and retrapping processes in moderately damped YBaCuO Josephson Junctions. Low Temp. Phys./Fizika Nizkikh Temperatur **39**, 378 (2013)
61. Tafuri, F., Massarotti, D., Galletti, L., Stornaiuolo, D., Montemurro, D., Longobardi, L., Lucignano, P., Rotoli, G., Pepe, G.P., Tagliacozzo, A., Lombardi, F.: Recent achievements on the physics of high-TC superconductor Josephson junctions: background, perspectives and inspiration. J. Supercond. Nov. Magn. **26**, 21 (2013)
62. Parlato, L., Arpaia, R., De Lisio, C., Miletto Granozio, F., Pepe, G.P., Perna, P., Pagliarulo, V., Bonavolont, C., Radovic, M., Wang, Y., Sobolewski, R., Scotti di Uccio, U.: Time-resolved optical response of all-oxide YBa2Cu3O7/La0.7Sr0.3MnO3 proximitized bilayers. Phys. Rev. B **87**, 134514 (2013)
63. Lombardi, F., Tafuri, F., Ricci, F., Miletto Granozio, F., Barone, A., Testa, G., Sarnelli, E., Kirtley, J.R., Tsuei, C.C.: Intrinsic d-Wave effects in YBa2Cu3O7-grain boundary Josephson junctions. Phys. Rev. Lett. **89**, 207001 (2002)
64. Miletto Granozio, F., Scottidi Uccio, U., Lombardi, F., Ricci, F., Bevilacqua, F., Ausanio, G., Carillo, F., Tafuri, F.: Structure and properties of a class of CeO2-based biepitaxial YBa2Cu3O7-Josephson junctions. Phys. Rev. B **67**, 184506 (2003)
65. We have assumed a mean values for London length λ_L of 300 nm, which is a value compatible with a GB angle of 20°
66. Papari, G., Carillo, F., Stornaiuolo, D., Longobardi, L., Beltram, F., Tafuri, F.: High critical current density and scaling of phase-slip processes in YBaCuO nanowires. Supercond. Sci. Technol. **25**, 035011 (2012)
67. Carillo, F., Papari, G., Stornaiuolo, D., Born, D., Montemurro, D., Pingue, P., Beltram, F., Tafuri, F.: Little–Parks effect in single nanoscale YBa2Cu3O6+x rings. Phys. Rev. B **81**, 054505 (2010)

68. Nawaz, S., Arpaia, R., Lombardi, F., Bauch, T.: Microwave response of superconducting YBa2Cu3O7-nanowire bridges sustaining the critical depairing current: evidence of Josephson-like behavior. Phys. Rev. Lett. **110**, 167004 (2013)
69. Scheible, D.V., Blick, R.H.: Silicon nano-pillars for mechanical single electron transport. Appl. Phys. Lett. **84**, 4632 (2004)
70. Scorrano, A., Carcaterra, A.: Semi-classical modelling of nanomechanical transistors. Mech. Syst. Signal Process. **39**, 489–514 (2013)
71. Scorrano, A., Carcaterra, A.: Investigation of nanomechanical transistors. Meccanica **48**(8), 1883–1892 (2013)
72. Rosi, G., Giorgio, I., Eremeyev, V.A.: Propagation of linear compression waves through plane interfacial layers and mass adsorption in second gradient fluids. ZAMM **93**(12), 914–927 (2013)
73. Placidi, L., Rosi, G., Giorgio, I., Madeo, A.: Reflection and transmission of plane waves at surfaces carrying material properties and embedded in second-gradient materials. Math. Mech. Solids, 1081286512474016, first published on March 4, 2013
74. Madeo, A., Gavrilyuk, S.: Propagation of acoustic waves in porous media and their reflection and transmission at a pure-fluid/porous-medium permeable interface. Eur. J. Mech. A/Solids **29**(5), 897–910
75. Alibert, J.J., Seppecher, P., Dell'isola, F.: Truss modular beams with deformation energy depending on higher displacement gradients. Math. Mech. Solids **8**(1), 51–73 (2003)
76. Pepe, G.P., Peluso, G., Valentino, M., Barone, A., Parlato, L., Esposito, E., Granata, C., Russo, M., De Leo, C., Rotoli, G.: Pulse-induced switches in a Josephson tunnel stacked device. Appl. Phys. Lett. **79**, 2771 (2001)
77. Dell'Isola, F., Vidoli, S.: Damping of bending waves in truss beams by electrical transmission lines with PZT actuators. Arch. Appl. Mech. **68**(9), 626–636 (1998)
78. Andreaus, U., Dell'isola, F., Porfiri, M.: Piezoelectric passive distributed controllers for beam flexural vibrations. J. Vib. Control **10**(5), 625–659 (2004)
79. Stornaiuolo, D., Rotoli, G., Massarotti, D., Carillo, F., Longobardi, L., Beltram, F., Tafuri, F.: Resolving the effects of frequency-dependent damping and quantum phase diffusion in YBa2Cu3O7-x Josephson junctions. Phys. Rev. B **87**, 134517 (2013)